J Bioenerg Biomembr (2012) 44:213–224
DOI 10.1007/s10863-012-9410-y

Subunit F modulates ATP binding and migration in the nucleotide-binding subunit B of the A_1A_O ATP synthase of *Methanosarcina mazei* Gö1

Devanathan Raghunathan · Shovanlal Gayen · Anil Kumar · Cornelia Hunke · Gerhard Grüber · Chandra S. Verma

Received: 22 November 2011 / Accepted: 8 January 2012 / Published online: 14 February 2012

Abstract The interaction of the nucleotide-binding subunit B with subunit F is essential in coupling of ion pumping and ATP synthesis in A_1A_O ATP synthases. Here we provide structural and thermodynamic insights on the nucleotide binding to the surface of subunits B and F of *Methanosarcina mazei* Gö1 A_1A_O ATP synthase, which initiated migration to its final binding pocket via two transitional intermediates on the surface of subunit B. NMR- and fluorescence spectroscopy as well as ITC data combined with molecular dynamics simulations of the nucleotide bound subunit B and nucleotide bound B-F complex in explicit solvent, suggests that subunit F is critical for the migration to and eventual occupancy of the final binding site by the nucleotide of subunit B. Rotation of the C-terminus and conformational changes in subunit B are initiated upon binding with subunit F causing a perturbation that leads to the migration of ATP from the transition site 1 through an intermediate transition site 2 to the final binding site 3. This mechanism is elucidated on the basis of change in binding affinity for the nucleotide at the specific sites on subunit B upon complexation with subunit F. The change in enthalpy is further explained based on the fluctuating local environment around the binding sites.

Keywords A_1A_O ATP synthase · Subunit B · ATP · Nuclear magnetic resonance (NMR) · Isothermal titration calorimetry (ITC) · Molecular dynamics simulations · Fluorescence correlation spectroscopy (FCS)

Abbreviations

FCS	Fluorescence correlation spectroscopy
MD	Molecular dynamics
NMR	Nuclear magnetic resonance
HSQC	Hetero nuclear single quantum coherence
ITC	Isothermal titration calorimetry
r.m.s.d.	Root mean square deviation
r.m.s.f.	Root mean square fluctuations
PCA	Principal component analysis
MM-GB-SA	Molecular Mechanics–Generalized Born–Surface Area enthalpy terms
Vdw	van der Waals

Introduction

Archaeal species have adapted to extreme environments with respect to temperature, salt concentration and pH

Electronic supplementary material The online version of this article (doi:10.1007/s10863-012-9410-y) contains supplementary material, which is available to authorized users.

D. Raghunathan · G. Grüber · C. S. Verma
Bioinformatics Institute (A*STAR),
30 Biopolis Street, #07-01 Matrix,
Singapore 138671, Singapore

D. Raghunathan
Now at Biosystems and Micromechanics,
Singapore-MIT Alliance for Research and Technology,
S16-07, 3 Science Drive 2,
Singapore 117543, Singapore

S. Gayen · A. Kumar · C. Hunke · G. Grüber (✉) · C. S. Verma
School of Biological Sciences, Nanyang Technological University,
60 Nanyang Drive,
Singapore 637551, Singapore
e-mail: ggrueber@ntu.edu.sg

C. S. Verma (✉)
Department of Biological Sciences,
National University of Singapore,
14 Science Drive 4,
Singapore 117543, Singapore
e-mail: chandra@bii.a-star.edu.sg

(Schäfer et al. 1999). One such example is the *Methanosarcina mazei* Gö1, which has provided scientists with a fine model system to study the atomic and molecular basis of the energy production and conservation in these organisms (Schäfer et al. 1999; Grüber and Marshansky 2008). It is known that the A_1A_O ATP synthase is the enzyme responsible for the synthesis of ATP from ADP and an inorganic phosphate in these organisms (Grüber and Marshansky 2008). This multi subunit enzyme with a proposed stoichiometry of A_3: B_3: C: D: E: F: G: H_2: *a*: c_x (Müller and Grüber 2003) is functionally related to the F_1F_O ATP synthase from eukaryotes and prokaryotes (Lolkema et al. 2003; Müller and Grüber 2003; Weber and Senior 2003) where three alternatively arranged subunits A and B contribute towards the water soluble A_1 domain (also referred to as the hexameric head), the primary site for ATP synthesis (Müller and Grüber 2003). The central stalk is made up of subunits C, D and F (Grüber et al. 2001). Subunit C has a funnel shaped structure with a central cavity, forming the space for the D and F assembly (Numoto et al. 2004). Subunit F in solution exhibits a distinct two-domain structure with the N-terminal having 80 residues and the residues 81-101 forming the flexible C-terminal part (Gayen et al. 2007). This C-terminal tail enables subunit F to undergo up and down movements relative to subunit B, bringing both termini in close proximity. The function of the central stalk is to connect as an elongated anchor, the hexameric headpiece A_1 and the membrane embedded A_O sector, allowing the energy to be transmitted by ion transduction from A_O to A_1 (Grüber et al. 2001). Our previous work (Gayen et al. 2007; Raghunathan et al. 2010) addressed the issue of coupling between the hexameric headpiece and the membrane integral A_O mediated via the stalk moiety. Employing fluorescence spectroscopy, NMR, molecular modeling, docking and molecular dynamics simulations, we proposed that the C-terminus of subunit F of the *M. mazei* Gö1 A_1A_O ATP synthase and the C-terminus of the nucleotide-binding subunit B of this enzyme specifically interact with each other, to partially accomplish coupling between the two motor elements A_1 and A_O. Having addressed "**How** does the coupling of A_1 and A_O motor elements take place?" (Raghunathan et al. 2010), we turn our focus to the question, "**Why** does the coupling of A_1 and A_O motor elements take place?"

The recently solved crystal structures of the nucleotide bound subunit B of the A_1A_O ATP synthase from *M. mazei* Gö1 revealed, how the ATP traverses the protein surface via two transient intermediate binding sites to its final binding pocket and the concomitant rearrangements in the nucleotide-binding and C-terminal region of subunit B (Kumar et al. 2008, 2009). In the present study, we combine this structural information with additional data derived from NMR, ITC, fluorescence spectroscopy experiments, molecular modeling; we draw on our previously proposed model of the subunit B-F complex (Raghunathan et al. 2010) to study the dynamics of the interactions of the nucleotide with subunit B and how this affinity is modulated in the presence of subunit F. Further, we comment on the change in structural dynamics in subunit B upon binding with subunit F that allows for the energetically favorable transition of the nucleotide from intermediate sites 1 and 2 and to the final binding site 3. Finally, we propose a model that places the interaction of subunits B, F and the nucleotide in the context of the larger A_1A_O ATP synthase assembly.

Material and methods

Biochemicals

Ni^{2+}-NTA-chromatography resin were received from Qiagen (Hilden, Germany);. Chemicals for gel electrophoresis were received from Serva (Heidelberg, Germany). Bovine serum albumin was purchased from GERBU Biochemicals (Heidelberg, Germany). The ATP- and ADP-analogues EDA-ATP ATTO-647N and EDA-ADP ATTO-647N were received from ATTO-TEC (Siegen, Germany). All other chemicals were at least of analytical grade and received from BIOMOL (Hamburg, Germany), Merck (Darmstadt, Germany), Roth (Karlsruhe, Germany), Sigma (Deisenhofen, Germany), or Serva (Heidelberg, Germany).

NMR spectroscopy

The C-terminal peptide $F_{81\text{-}101}$ of the *M. mazei* Gö1 subunit F was synthesized and purified as described recently (Raghunathan et al. 2010). A series of ^1H-^{15}N HSQC spectra of $F_{81\text{-}101}$ were recorded at different concentrations of ATP. 2 mM of unlabelled peptide was used for the reference spectrum. The nucleotide was added in increasing amounts to a molar ratio of 1:1 to 1:5 and chemical shift perturbations were monitored in the ^1H ^{15}N HSQC spectrum. Experiments were performed on a Bruker Avance 600 MHz machine using Topspin for acquisition and processing of spectra. Respective spectra were overlapped to monitor chemical shift changes; further analysis was done in SPARKY (Kneller and Goddard 1997).

Determination of nucleotide binding to subunit F by fluorescence correlation spectroscopy

Fluorescence correlation spectroscopy was performed on an LSM 510 Meta/ConfoCor 3 (Zeiss, Jena, Germany) using the fluorescently labelled ATP analogue EDA-ATP ATTO-647N (ATTO-TEC, Siegen, Germany). For the FCS experiment

50 mM Tris/HCl (pH 8.5) with 150 mM NaCl buffer was used. The temperature was adjusted to 25 °C in an incubation chamber (Zeiss). The 633 nm laser line of a HeNe633 laser were attenuated to 5 mW and focused into the aqueous solution by a water immersion objective (40 ×/1,2 W Korr UL-VIS-IR, Zeiss). FCS was measured in 15 μl droplets of the diluted fluorescent derivatives of ATP, which were placed on Nunc 8 well chambered cover glass. Before usage, the cover glasses were treated with 3% of gelatin, in order to prevent unspecific binding and removed by washing steps with H_2O (Hunke et al. 2007). Following filter sets were used: MBS: HFT 514/633, EF1: BP 655-710 IR, EF: None, DBS: None. Out-of-focus fluorescence was rejected by a 90 μm pinhole in the detection pathway. Solution of Cyanine 5 in water was used as references for the calibration of the confocal microscope. Variable concentrations of protein solutions were mixed after addition of $MgCl_2$ and fluorescently labelled nucleotide. The drops were incubated on the glass slip surface for 3 min, and monitored during this time by FCS. The fluorescence autocorrelation functions were determined by measurements of at least 10 repetitions with 30 s each. ConfoCor 3-software 4.2, Excel 2003 and OriginPro 8 SR4 were used to calculate the bound fractions and the dissociation constants. A 'Standard AC normalized triplet' model was used to determine the diffusion time of the fluorescently nucleotides. The determined value was fixed for the fitting in the titration experiments, whereby the 'Standard AC2 diffusion coefficients normalized triplet' model has been used, which takes two components into consideration. The second parameter was determined and fixed during the calculations to determine the bound fractions and autocorrelation functions, which were analyzed in Microsoft Excel and the figures, generated in OriginPro 8. The resulting sigmoidal non-linear curve fit was used to calculate the binding constant.

Intrinsic tryptophan fluorescence measurements

A *Varian Cary Eclipse* spectrofluorimeter was used, and all experiments were carried out at 20 °C. The intrinsic tryptophan of $F_{81\text{-}101}$ was excited at 295 nm, and the emission was recorded from 310 to 380 nm with excitation and emission band passes set to 5 nm. For titration of the tryptophan fluorescence of peptide $F_{81\text{-}101}$ with ATP, the emission wavelength was 338 nm. Before use, peptide $F_{81\text{-}101}$ and increasing amounts of ATP were incubated in a buffer of 50 mM Tris/HCl (pH 8.0) for 5 min.

Isothermal titration calorimetry (ITC)

Mg-ATP was titrated against 15 μM of *M. mazei* Gö1 $F_{81\text{-}101}$ in a VP-ITC micro-calorimeter (Microcal, Northampton, UK). $F_{81\text{-}101}$ was maintained in sodium phosphate buffer (pH 6.5) at 25 °C and titrated in steps of 10 μl. The heat of dilution, determined by titrating Mg-ATP into buffer, was subtracted from the raw data before curve fitting and refinement. The dissociation constant of Mg-ATP to $F_{81\text{-}101}$ was determined by least squares method and the binding isotherm was fitted using Origin v7.0 (Microcal) assuming a single-site binding model.

Molecular modeling and dynamics

The preparation of the initial *M. mazei* Gö1 subunit B-F complex has been described in detail in our previous paper (Raghunathan et al. 2010). The binding mode of ATP at transition states 1, 2 and final binding site 3 were carefully reconstructed on the subunit B and the complex of B-F based on the crystal structures. Molecular dynamics simulations (MD) were carried out for 1) ATP bound to subunit B as captured in transition states I and II as well as in its final binding position III and, 2) ATP bound to the complex of subunits B and F, resulting from the docking at transition states I and II as well as in its final binding position III; this resulted in a total of six MD simulations of 10 ns each. Further, MD simulations on a model system of ATP bound to the $F_{81\text{-}101}$ as predicted by NMR, ITC and fluorescence spectroscopy were carried out.

For each system, the minimization, equilibration and simulation procedures were as outlined earlier (Raghunathan et al. 2010). Briefly, molecular dynamics simulations in explicit solvent conditions employing the TIP3 (Jorgensen et al. 1983) model of water were conducted using the CHARMM force field (MacKerell et al. 2000; Mackerell 2004; Mackerell and Nilsson 2008) employing the NAMD (Phillips et al. 2005) package. The electrostatic interactions were modelled using the particle mesh Ewald (Darden et al. 1993) summation method and the van der Waals energies were computed using a smooth (10–12 Å) cutoff. Following minimization, heating and equilibration, production runs over 10 ns in the NpT ensemble using the Nose-Hoover Langevin piston pressure control (Martyna et al. 1994; Feller et al. 1995) in NAMD were performed. The trajectories were analyzed using CHARMM (Brooks et al. 2009) and Wordom (Seeber et al. 2007). Clustering was implemented in the statistical package R (R Development Core Team 2008) and all pictures were made using PyMOL (DeLano 2002).

The binding enthalpies of ATP binding to the proteins (in the presence of Mg^{2+}) were determined using the MM-GB-SA methodology (Srinivasan et al. 1998; Kollman et al. 2000). While the simulations are indeed carried out in explicit solvent where the electrostatics is modeled by the particle mesh Ewald method, these results in energy terms that are not pair wise additive and hence reveal no details on the interaction between selected residue pairs. The application of the post-processing MM-GB-SA technique involves calculation of various energy terms contributing to the enthalpy of binding such as electrostatics, determined under

the Generalized Born approximation which makes it possible to study the interaction profiles between residue pairs. The enthalpy of binding, ΔH is inherently composed of two terms 1) the change in molecular mechanics (MM) free energy upon complex formation denoted by ΔH_{MM} and 2) the enthalpic contribution arising as a result of solvation denoted by ΔH_{solv}. The molecular mechanics term is further decomposed into a van der Waals and a Coulomb term ($\Delta H_{MM} = \Delta H_{vdW} + \Delta H_{elec}$), while the solvation term is further divided into a polar and non-polar component ($\Delta H_{solv} = \Delta H_{polar\text{-}GB} + \Delta H_{non\text{-}poloar\text{-}SA}$). The GBSW (Im et al. 2003) module as implemented in CHARMM was employed to evaluate the (Generalized Bonn GB approximation) polar component of ΔH_{solv} while the non-polar component was evaluated from the solvent accessible surface area (SA) using a probe radius of 1.4 Å according to the equation $\left(\Delta H_{non-poloar-SA} = \gamma \Delta SA + \beta\right)$, where γ, the macroscopic surface tension coefficient and β, the offset were set to their standard values of 0.00542 kcal mol^{-1} $Å^{-2}$ and 0.92 kcal/mol (Sharp et al. 1991; Sitkoff et al. 1994). Additionally, the temperature was set to 300 K and the salt concentration was set to 0.15 M.

Given the prohibitively large sizes of the complex (~550 residues), the entropic aspects of the binding process cannot be adequately addressed using molecular dynamics simulations. This is because the common methodology adopted is to either computing the vibrational or less commonly, the quasi-harmonic entropies (Levitt et al. 1985; Chang et al. 2005). The vibrational entropy requires the diagonalization of the Hessian, which is the matrix of the second derivatives of the potential energy with dimensions 3 N*3 N (N being the number of atoms) and can become huge as the number of atoms in a system increases. Here we attempt to correlate the enthalpic component of the binding energy with that inferred from experimental techniques.

Results and discussion

Structure, dynamics and thermodynamics of the subunit F-ATP complex

The solution structure of $F_{81\text{-}101}$ exhibits a defined loop formation at it's very N-terminus (Raghunathan et al. 2010), being part of the glycine rich sequence $_{78}$GCSGSGSTS$_{86}$, reflecting a phosphate loop (P-loop) motif GXXGXGKTV (Walker et al. 1982). Surface representation of the NMR structure shows the presence of both positive and negatively charged surface areas. Residues Arg88, Lys92 and Lys101 form the positively charged area; residues Glu89 and Asp98 formed the negatively charged surface area (Fig. 4 in (Raghunathan et al. 2010)). Zero-length cross-link data (Schäfer et al. 2006a, b) and intrinsic tryptophan fluorescence spectroscopy (Gayen et al. 2007) showed that the association of subunit B and subunit F occurs via the C-termini of both subunits. Thus, it might be possible that cationic regions on the extended C-terminus of subunit F may interact with the anionic patches on the ventral face of B.

To study the nucleotide-binding features of subunit F, fluorescence correlation spectroscopy (FCS) using fluorescently labelled ATP and ADP was performed. As a reference, the mean count rate per Cyanine 5 (Cy5) fluorophore was determined to be 79.9±0.2 kHz. The fluorescent nucleotide derivatives MgATP ATTO-647N and MgADP ATTO-647N showed a mean count rate of 38.3±1.5 kHz and 19.8±2.1 kHz. The characteristic diffusion times for Cy5 (59.6±1.6 μs) MgATP ATTO-647N (84.3±3.3 μs) and MgADP ATTO-647N (80.1±4.5 μs) were determined by fitting the autocorrelation functions. The autocorrelation curves of the fluorescent nucleotide analogues and the increased concentrations of subunit F are shown in Fig. 1. The increase of the mean diffusion time τ_D was due to the increase in the mass of the diffusing particle, when fluorescently labelled nucleotide interacts with subunit F. Binding constants of 455.6±3 μM for Mg-ATP and 449.0±2 μM for Mg-ADP were determined (Fig. 1).

$F_{81\text{-}101}$ forms the nucleotide-binding epitope in subunit F

To prove, whether the C-terminal region of subunit F, $F_{81\text{-}101}$, which includes the glycine rich sequence $_{78}$GCSGSGSTS$_{86}$, is able to bind ATP, ^{1}H-^{15}N HSQC experiments were done in the absence and presence of different concentration of the nucleotide. An overlaid ^{1}H-^{15}N HSQC spectra of $F_{81\text{-}101}$ in the absence and presence of increasing concentration of ATP is shown in Fig. 2a. With the addition of ATP, the maximum chemical shift change occurs for residues Gly83, Ser84, Thr85, Val95, Val97, Trp100 and Lys101, whereas residues Leu87, Arg88, Glu89, Asp98 and Leu99 have medium chemical shift change and residues Ser86, Lys90, Ile91 and Ala94 have no or minimum chemical shift change. The change of peak position can occur due to ATP binding as well as binding induced conformational change. A model fitting of ATP into the $F_{Mm\ (81\text{-}101)}$ structure reveals close contacts of the nucleotide to the P-loop as well as cation-π and π-π* interaction of Arg88 and Trp100 with the adenine-ring, respectively (Fig. 2b). α-, β- and γ-phosphate are in close proximity to the residues Ser84, Thr85 and Ser82 with distances of distance 3.04 Å, 2.30 Å and 4.02 Å, respectively.

Since the NMR-titration experiment of $F_{81\text{-}101}$ with ATP has shown that the only tryptophan residue (Trp100) of the peptide undergoes a shift in the HSQC spectra after addition of ATP, we used intrinsic tryptophan fluorescence spectroscopy to confirm and to quantitatively evaluate the binding of the nucleotide to the $F_{81\text{-}101}$. The corrected

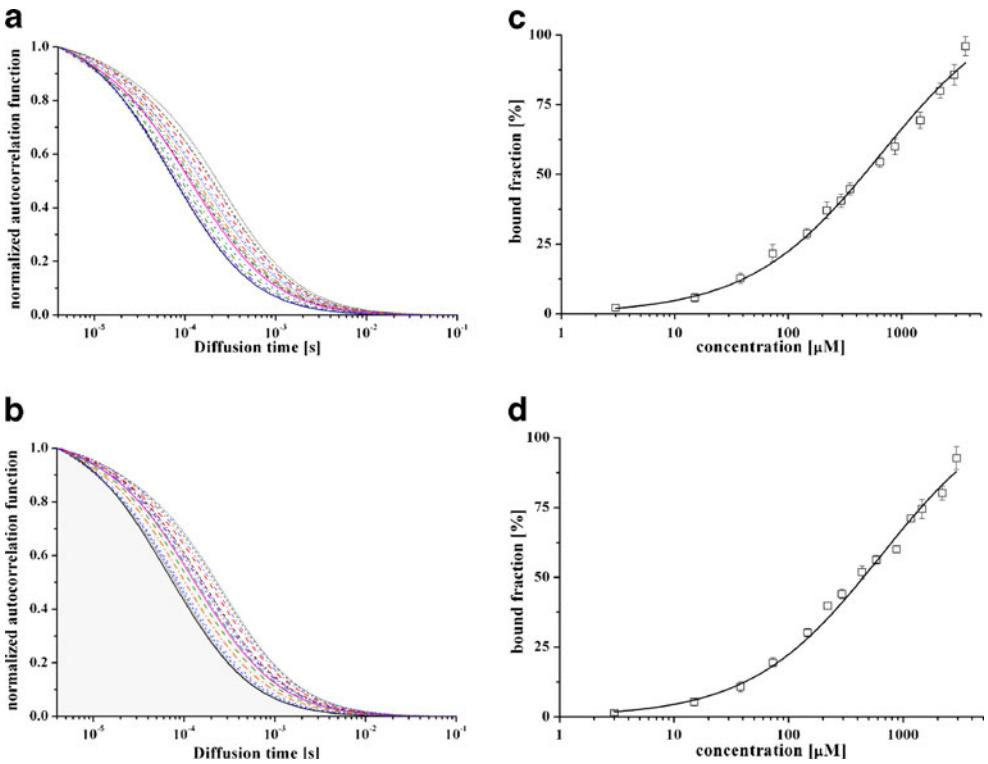

Fig. 1 Determination of the binding traits of subunit F to fluorescently labelled nucleotides via FCS titration experiments. Normalized autocorrelation functions of MgATP ATTO-647N (**a**) and MgADP ATTO-647N (**b**) alternatively obtained by increasing the quantities of subunit F. Concentration dependent binding of binding of MgADP ATTO-647N (**c**) and MgATP ATTO-647N (**d**) alternatively to subunit F. The best fit to titration curves are shown as a non-linear, Hill curve fit

tryptophan fluorescence spectrum of $F_{81\text{-}101}$ reveals the emission maximum of the peptide at 339 nm (data not shown). The intensity dropped by 21% after addition of ATP, indicating that the significant drop in fluorescence is also caused by the interaction of Trp100 and the nucleotide. To quantitate the spectra, the binding of ATP to $F_{81\text{-}101}$ was measured using fluorescence quenching at 339 nm, and the result is presented in Fig. 2c. The titration curve has a hyperbolic shape from which a binding constant (K_D) of 560 µM could be determined. In a second quantitative approach using isothermal titration calorimetry the profile (Fig. 3) for Mg-ATP binding to $F_{81\text{-}101}$ gives a negative free energy change (ΔG (kcal/mol) = −4.26) for the binding reaction and suggests that the overall reaction is favourable. The curve fitting was done using a one site model (Fig. 3). The K_D was calculated to be 510 µM and thus is in accordance with the fluorescence experiment. Furthermore, the data demonstrate that $F_{81\text{-}101}$ is the segment of subunit F, enabling this stalk subunit to bind nucleotides. The number of binding sites (N), enthalpy (ΔH) and entropy (ΔS) changes of the binding event were calculated as: N=1, ΔH (kcal/mol) = −26.1±3.8, TΔS (kcal/mol) = −21.9, respectively. A fitting of ATP into the $F_{81\text{-}101}$ structure reveals close contacts of the nucleotide to the phosphate loop (P-loop) as well as cation-π and π-π (Dougherty 1996; Gallivan and Dougherty 1999; Dougherty 2007) interaction of Arg88 and Trp100 with the adenine-ring, respectively (Fig. 2b). Taken together, these studies collectively draw on four different biophysical techniques viz. fluorescence correlation-, NMR and intrinsic tryptophan fluorescence spectroscopy and isothermal calorimetry to unambiguously show that subunit F as well as the peptide do bind to the nucleotide. These results confirm previous data, revealing that peptides with only 12 residues in length are able to bind and recognize ATP in water (Butterfield and Waters 2003).

To validate the proposed model of binding of ATP to the P-loop motif of $F_{81\text{-}101}$; the free energy of binding of ATP to the $F_{81\text{-}101}$ in the model constructed above, was determined from an 8 ns molecular dynamics trajectory using the MM-GB-SA approach as described in the methods section. The computationally determined value of ΔH = −27.7±2.8 kcal/mol (the energy components are summarized in Table S1) is close to the experimentally determined value.

The vibrational entropy was further evaluated by analysing the normal modes of the system (Brooks and Karplus 1983). Upon performing NMA, the entropy of binding was determined to be 25.1±7.5 kcal/mol.

The value of entropy thus determined is within the error limits of the value obtained from experiments (−21.9 kcal/mol). The entropy of larger systems is notoriously time and memory demanding. Given the prohibitively large sizes of the *M. mazei* Gö1 subunit B and the subunit B-F complex, the entropic aspects of the binding cannot be easily addressed using molecular dynamics simulations and hence excluded from the current study.

At the structural level, the MD trajectory reveals that the ATP binds to $F_{81\text{-}101}$ with the adenine ring sandwiched

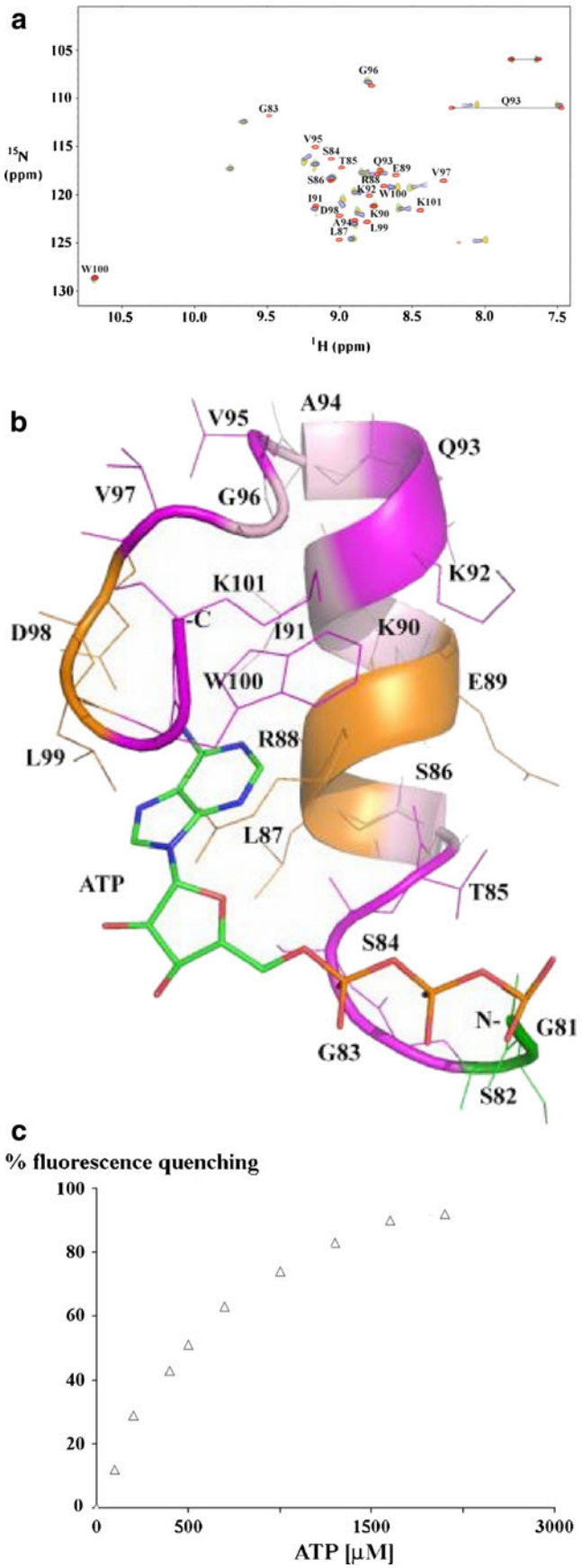

◀ **Fig. 2** **a** Overlay of 2D ^{1}H-^{15}N-HSQC spectra of F_{81-101} from *M. mazei* Gö1 in the absence (*red*) and presence (*blue, yellow and green*) of 8.33 mM, 16.6 mM and 30 mM Mg-ATP. The spectrum was collected in a Bruker Avance 600 MHz spectrometer at 25 °C. **b** ATP binding model for the peptide: *pink*, *orange* and *light pink* colour residues represent the maximum, medium and no/minimum chemical shift change respectively in the HSQC spectrum upon ATP addition. **c** Intrinsic tryptophan fluorescence titration of F_{81-101} with ATP. Excitation was at 295 nm and the emission was measured at 339 nm

between the residues Arg88 and Trp100, while the phosphate moiety interacts with Ser84. A breakdown of the enthalpy into its components shows that while there is a significant electrostatic interaction between the ATP and subunit F, nevertheless, the burial of the charged groups involved in making these interactions incurs a high penalty of desolvation, with the result that the binding is driven by van der Waals interactions. The close agreement of the enthalpic component of the binding affinity derived from our computational studies with the binding enthalpy measured from experiments supports the fact that the MM-GB-SA protocol thus designed is appropriate for the purposes of this study.

Dynamics of the B-ATP complex and binding profile of ATP at sites 1, 2 or 3

It has been hypothesized (Kumar et al. 2008; Manimekalai et al. 2009) that the binding of ATP to subunit B of the *M. mazei* Gö1 A-ATP synthase goes through two intermediate states (site 1 and site 2) to its final binding site 3 (Fig. 4a). The two intermediate states have been identified using crystallography and fluorescence spectroscopy (Kumar et al. 2008, 2009; Manimekalai et al. 2009); however the complex with the final binding site occupied is yet to be resolved. Nevertheless, it is reasonable to assume that the final binding site of the nucleotide in subunit B would mimic that of the known nucleotide binding site in the homologous α subunit of F_1F_O ATP synthase, because of the highly conserved nature of the residues in the binding pocket and the overall similarity in structure and the mapped covalently bound nucleotide analogue in subunit B of the *M. mazei* Gö1 A_1A_O ATP synthase (Schäfer et al. 2006a, b).

The B-factors (Willis and Pryor 1975) of the C-alpha atoms (Figure S1) give an indication of the fluctuations experienced by the subunit B protein in the crystal structures (free form, with ATP bound at site 1 and with ATP bound at site 2). Figure S2a describes the fluctuations along the trajectory as experienced by each residue of subunit B (when not complexed with subunit F), when the nucleotide is bound to sites 1, 2 or 3. The residues that undergo major changes (localized in the C-terminal region) are shown in figure S3 (black line). It is clear that regions that are distant from the nucleotide binding sites also undergo perturbations

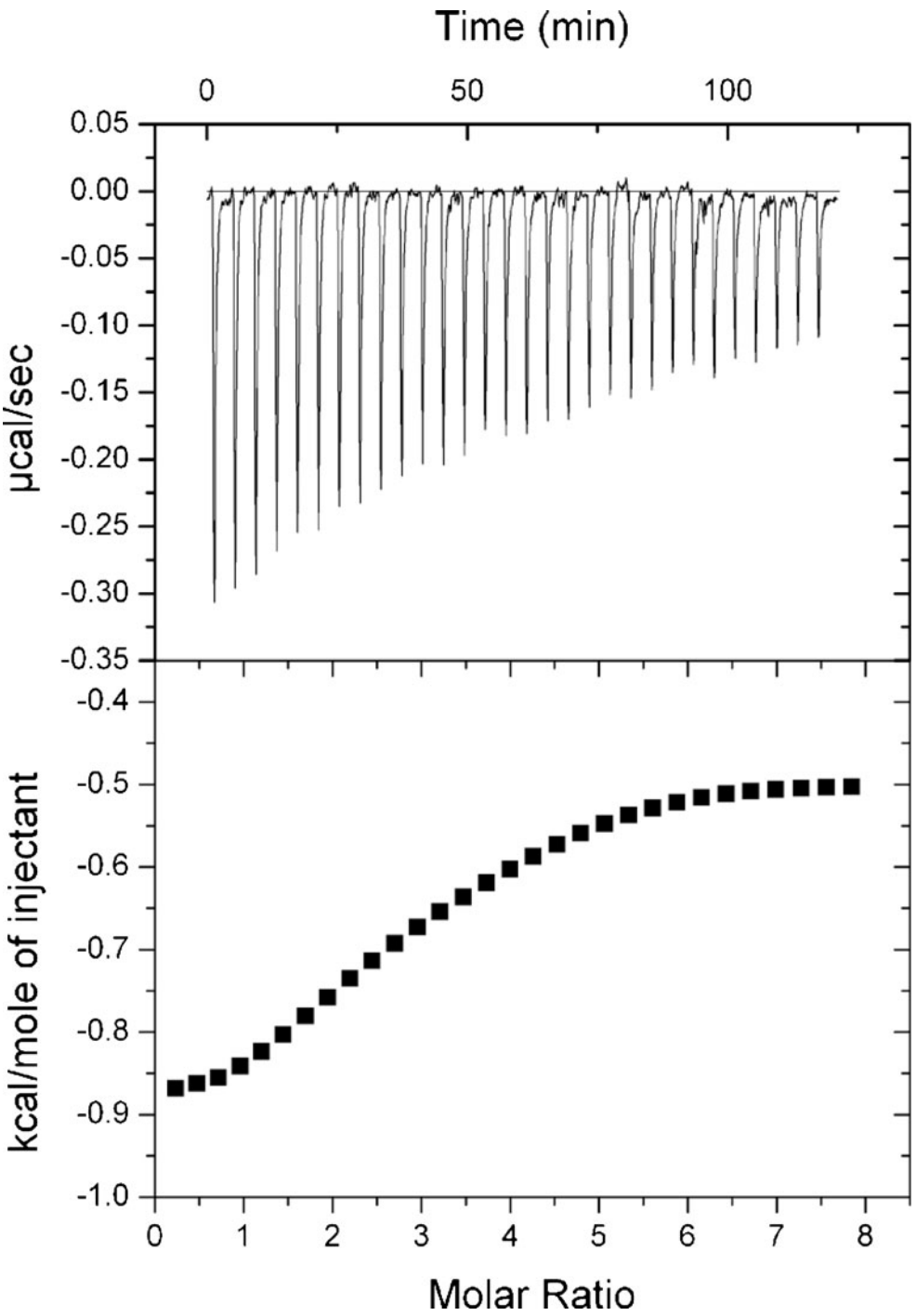

Fig. 3 Binding affinity measurements for $F_{81\text{-}101}$ with Mg-ADP using ITC: The top panel of the figure shows the injection profile after baseline correction and the bottom panels show the integration (heat release) for each injection. The bottom panel shows the fit of the data to a function based on a one-site binding model

and are mostly charged residues; this is not surprising given that the nucleotides are highly charged. The region near residues 268-270, undergoing large fluctuations, is a loop with Arg and Gly residues that clearly respond to the presence of the charged nucleotides, despite being distant from the binding sites. The changes highlighted (by black arrows) allude to the fact that major fluctuations, indicative of local dynamics, occur only when the nucleotide inhabits site 1 or site 2. The nucleotide bound at site 3 does not instigate large fluctuations on the surface of subunit B.

The MD trajectories further reveal that the nucleotide adopts multiple binding modes at the intermediate sites 1 and 2 (Fig. 4b A1, 4B1), characterized by a large degree of both rotational and translational motions. However, the nucleotide binding mode at site 3 is highly clustered (Fig. 4b C1). The observation of multiple binding modes of the nucleotide at sites 1 and 2 and higher degree of fluctuation of residues on subunit B associated with these two binding sites is in accord with the observation that the nucleotide locations at site 1 and site 2 are captured

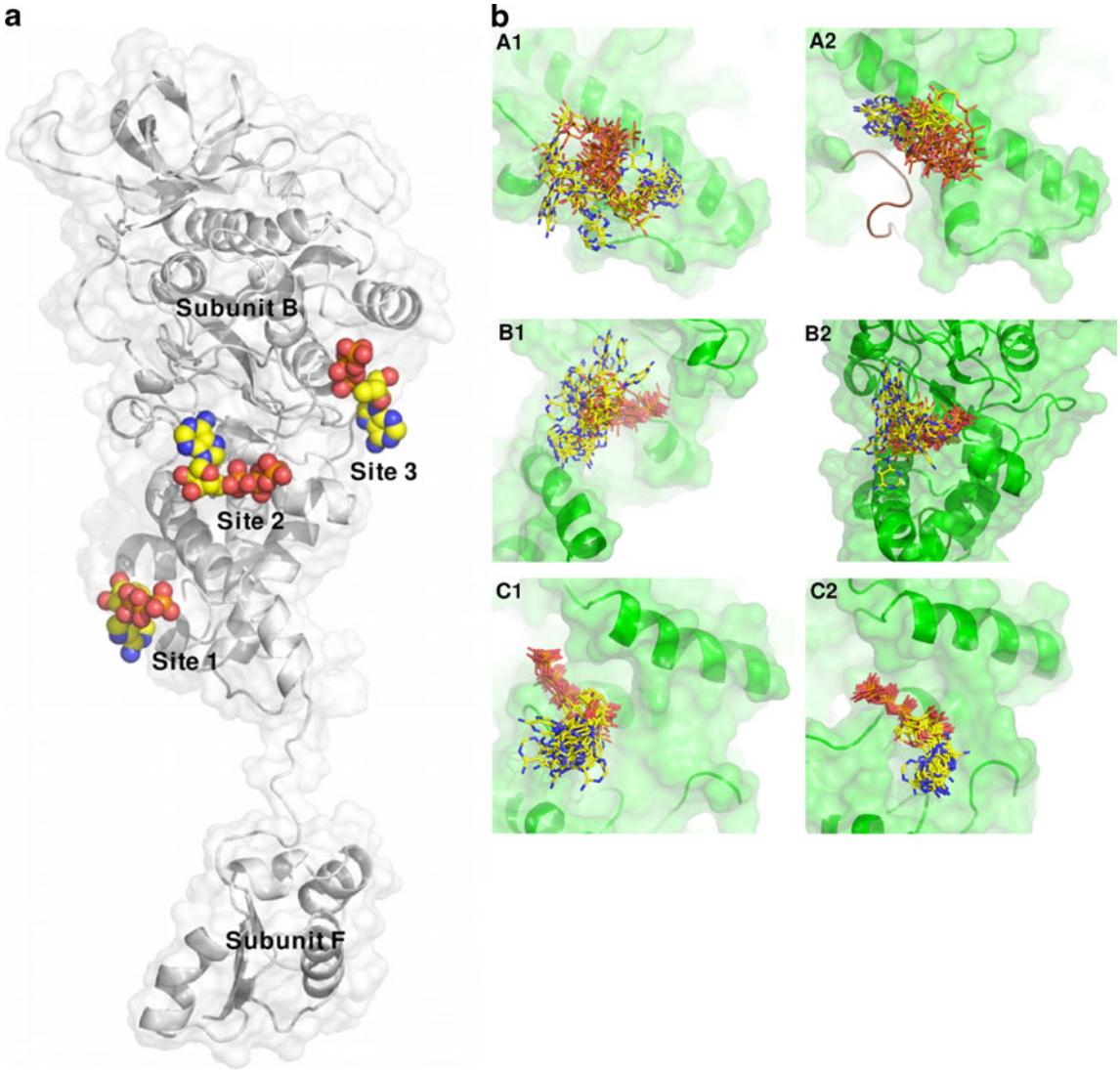

Fig. 4 Structure of *M. mazei* Gö1 subunit B complexed with F shown in cartoon representation with translucent surface (*white*). The ATP at transition site 1, site 2 and final nucleotide binding position 3 are indicated in spheres. On the right, ensemble of binding modes of ATP with respect to subunit B obtained after clustering. A1, B1 and C1 denote the binding modes of ATP on subunit B in the absence of subunit F while A2, B2 and C2 depict the binding modes of ATP on subunit B in the presence of subunit F

as transient intermediates in the crystal structures (Kumar et al. 2008, 2009; Manimekalai et al. 2009). Further, the decreased fluctuations on subunit B, when the nucleotide is bound at site 3 is combined with the observation of a tighter binding mode adopted by ATP, substantiates our assumption of site 3 as the final binding site of ATP on subunit B.

To gain a quantitative insight into the energetics as well as the conformational changes accompanying the binding of the nucleotide at the two intermediate sites and the final binding site on subunit B, we have computed the enthalpic component that drives the association of the nucleotide to subunit B using MD simulations.

Given the variance in binding modes of ATP, we compute the binding energetics of the nucleotide after adopting a clustering scheme as shown in figure S4 (based on the measurement of critical dihedral angles as well as the distance between the P_γ of the ATP and the residue on subunit B that contributes maximum towards its affinity), that allowed for the identification of structures that most accurately reflect the multiple binding modes (Fig. 4b A1 to C2). The probability of the nucleotide adopting a certain binding mode was reflected by the cluster size. The enthalpy thus obtained by clustering and then summing over the population of each cluster could be a more realistic reflection of the underlying process of nucleotide binding and would better reflect the affinity of ATP towards the particular site (in contrast to taking an average over the trajectory). The binding mode of ATP at site 3 (Fig. 4b C1) is much less proliferated as compared to the modes adopted at site 1

and site 2. However, the clustering algorithm was adopted to estimate the binding enthalpy at site 3 as well. Table S1 reveals that the binding affinity of ATP for subunit B follows the trend: site 2 (−47.4) > site 3 (−31.9) > site 1 (−16.1). A residue wise decomposition of the interaction energy reveals that the binding of nucleotide to subunit B at site 2 is mainly driven by electrostatic interactions with the side chains of residues Arg334*, Arg379, Lys335* and Arg382. This is followed by site 3, where residues Arg334*, Arg330* and Arg413 contribute towards nucleotide affinity. Finally, residues Arg443*, Lys365*, Arg349* and Arg396 contribute the most at site 1. The residues marked with the superscript (*) are highly conserved across the homologues of subunit B in the A- and F- ATP synthases as well as V-ATPases (Fig. 7 described in Kumar et al. 2009).

Dynamics of the subunit B-F-ATP complex and binding profile of ATP at site 1, 2 or 3

Figure S2b and figure S3 (red line) describes the fluctuations along the trajectory as experienced by each residue of subunit B (complexed with subunit F) when the nucleotide is bound at site 1, site 2 or site 3. It is interesting to note that the residues on subunit B become sequestered when nucleotide binds at site 1 and 3 in the presence of subunit F. However, the presence of subunit F causes prominent fluctuations in the residues between 260 to 280, 340 to 360 and 380 to 400 (indicated by arrows). These regions are either in the vicinity of the nucleotides at site 1 and site 2 or are in the flexible and charged 268-270 loop region. Barring the variability in the r.m.s.f. for residues between 340 and 360 when nucleotide is bound at site 1, the residues on subunit B appear to consistently experience enhanced fluctuations when the nucleotide is bound at site 2 (Fig. S3). Nucleotide binding at site 3 causes least perturbations to the residues of subunit B. Interestingly, the network of residues that exhibit enhanced fluctuations and interactions when nucleotide is bound at site 1 or site 2 (Fig. S2 and S3) suggests the occurrence of an asymmetry in perturbations, that ensures a directionality for the movement of nucleotide from site 1 towards site 2 (Fig. S5a) and from site 2 towards site 3 (Fig. S5b).

Next, we enquire into the nucleotide affinities at the three sites of subunit B in the presence of subunit F. A clustering scheme (Fig. S4), as described in the previous section was adopted, to identify the most probable binding modes. The resulting enthalpy of binding (in kcal/mol) reveals that ATP affinity for subunit B (Table S1) follows the trend in kcal/mol: site 3 (−45.3) > site 2 (−33.6) > site 1 (−20.9). This switch to site 3, being the highest affinity site in subunit B in the presence of subunit F, suggests that conformational changes in subunit B are important for this to occur. Residue wise decomposition of the interaction energies reveals that binding of nucleotide to subunit B at site 3 is mainly driven by electrostatic interactions between the charged phosphate of the ATP and the backbone of Asp158, Asn157 and His156. Further, stacking between Trp416 and Tyr338 and the adenine moiety of the ATP contributes to the π-π interactions. This is also reflected in the favourable van der Waal component of binding at site 3 in the presence of subunit F (−7.7 kcal/mol). Finally, an Mg^{2+}-mediated interaction between Glu189 and the phosphate tail of ATP is noted. This is followed by site 2, where interactions between side chain of Arg330 and phosphate of ATP, side chain of Gln325 and ATP N6 and Mg^{2+}-mediated interactions between the ATP phosphate and Val328 and Ser150 backbone contribute towards nucleotide affinity. Finally, Mg^{2+}-mediated interaction between the phosphate and Gly377 and polar contacts between the phosphate of ATP and Arg396 hold the ATP at site 1.

Collectively, the structural and thermodynamic investigations reveal that subunit F, when complexed with subunit B has a twofold effect; (a) at the structural level, it amplifies the fluctuations on subunit B in the vicinity of nucleotide binding site 2 and (b) at the thermodynamic level, the affinity of nucleotide for subunit B shifts towards the final binding site 3 with a decrease in the affinity at site 2.

Implications on nucleotide affinity when subunit F binds to subunit B

Figure 5 suggests that the incoming subunit F upon complexation with the C-terminus of subunit B shifts

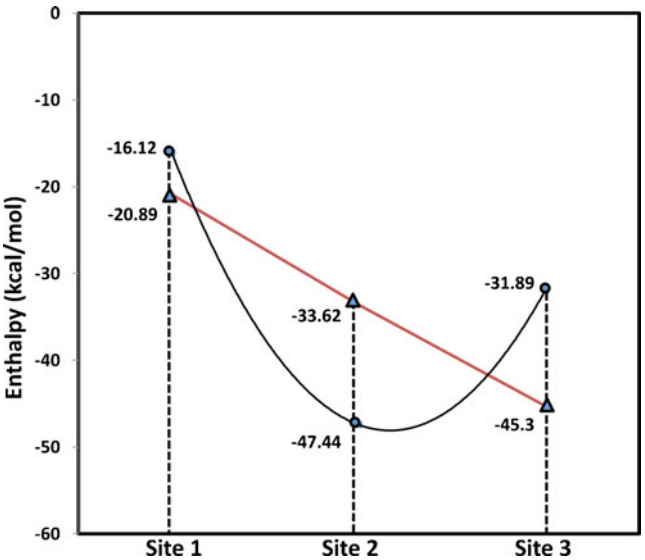

Fig. 5 The change in enthalpic component of the binding affinity of the ATP to *M. mazei* Gö1 subunit B plotted as a function of the binding site obtained from the optimized MM-GB-SA protocol applied to a 10 ns molecular dynamics trajectory. The *black line* indicates the enthalpy trend, when subunit B is uncomplexed, while the *red line* indicates the binding trend of ATP to subunit B in the presence of subunit F

the propensity of nucleotide binding towards site 3. This is achieved by a simultaneous increase in enthalpic affinity of nucleotide at site 1 ($\Delta\Delta H$ = 4.8 kcal/mol) and site 3 (where $\Delta\Delta H$ = 13.4 kcal/mol), while the enthalpic component of binding is destabilized by ~14 kcal/mol at site 2 of subunit B upon subunit F binding. Principle component analysis (Fig. S6) provides further evidence that the nucleotide binding is "tightened" at sites 1 and 3 upon subunit F interaction, while the increase in scatter in the PC1 vs. PC2 is indicative of a "loosening" of the affinity at site 2 (Fig. S6).

These simulations suggest that the binding of subunit F to subunit B facilitates the migration of ATP towards its final binding site 3 by causing a local perturbation that in turn leads to a decrease in the enthalpic binding affinity at site 2 and a substantial increase in the binding of ATP at site 3 (and site 1). The difference in these affinities provides a gradient that allows for a smooth transition from site 1 to site 2 and finally to site 3 in the presence of subunit F (red line in Fig. 5). In contrast, our data indicate that, if subunit F was not to bind to subunit B, the nucleotide would be caught in a transient binding mode at site 2 and would be incapable of transitioning to its final binding site 3 (black line in Fig. 5).

Interactions of $F_{81\text{-}101}$ with subunit B in the presence of ATP at sites 1, 2 or 3

In a previous work, we employed restraint based docking to propose a model of the B-F assembly based on experimental distance restraints derived from intrinsic fluorescence spectroscopy and biochemical cross linking (Schäfer et al. 2006a, b; Gayen et al. 2007). Intrinsic tryptophan fluorescence spectroscopy placed Trp100 of the *M. mazei* Gö1 subunit F in the vicinity of Trp430 of subunit B. Further, biochemical cross linking placed the stretch of residues $_{88}$REKIK$_{92}$ on F close to the region spanning $_{390}$EALSERDTK$_{398}$ of subunit B. These regions continue to make productive contacts that confer structural stability to the B-F complex in the presence of the nucleotides at the three sites. We used two measures to probe the interactions between the C-terminal region of subunit F and subunit B with the nucleotide occupying one of the possible three sites described earlier. At the thermodynamic level, we calculated the binding enthalpy between these regions (Table S2) and at the structural level, we monitored the distribution of the C-alpha distances between the regions $F_{81\text{-}101}$ and subunit B over the entire trajectory (Fig. S7) for the three cases. The enthalpy data as summarized in Table S2 reveals that the binding enthalpy between $F_{81\text{-}101}$ and subunit B is enhanced, when the nucleotide occupies sites 2 and 3. While the binding at site 3 is more electrostatically driven, the binding at site 2 is determined by the packing environment as suggested by the favourable van der Waals term. In contrast, $F_{81\text{-}101}$ exhibits a reduced affinity for subunit B when the nucleotide occupies site 1. A combined effect afforded by a less favorable electrostatic term (compared to site 3 case) and adverse packing (compared to site 2) accounts for this decrease. Figures S8 and S9 describe the residue wise decomposition (at the C-termini of subunits B and F) of the electrostatic and van der Waals components of the interaction energy. At the structural level, the distribution of C_α distances between $F_{81\text{-}101}$ and

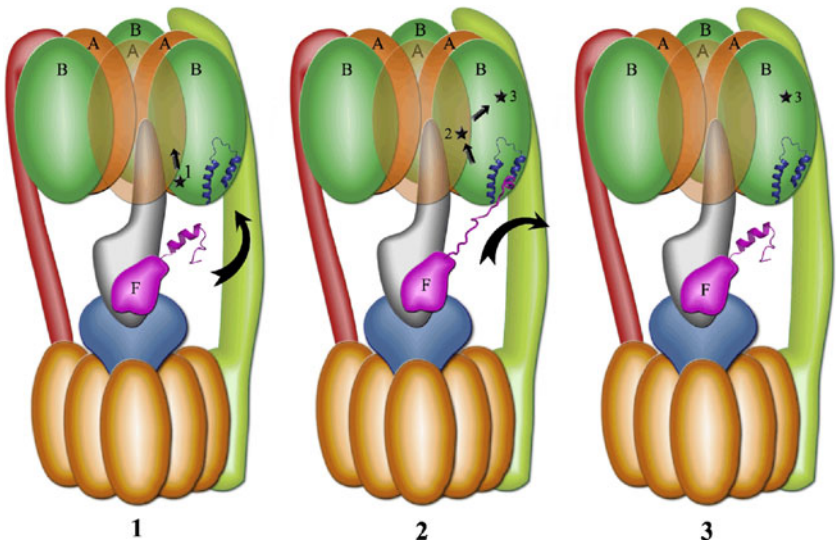

Fig. 6 Schematic representation of the effect of *M. mazei* Gö1 subunit F binding to subunit B. Three stages are described; firstly in stage 1, the retracted C-terminus of subunit F elongates to make productive contacts with the C-terminus of subunit B. This initiates the migration of ATP from site 1 towards site 2. Next in stage 2, the binding of subunit F to subunit B is enhanced, simultaneously resulting in the migration of ATP from site 2 towards site 3. Finally in stage 3, after ATP has occupied its final binding site 3, the C-terminal region of subunit F unbinds from the C-terminus of subunit F and readopts a retracted, helical structure

subunit B suggests a higher degree of closeness, when the nucleotide is bound at site 2. This distribution suggests that in the presence of an occupied site 2, the two subunits come closest to each other and may enable the nucleotide to migrate to site 2 or to site 3, exhibiting a transient state like character. Of course, the enthalpy of binding to site 1 is weakened by ~5 kcal/mol when the two subunits are together, while that at site 3 is strengthened by ~13 kcal/mol, thus suggesting that the nucleotide will migrate preferentially to site 3.

Taken together, it is conceivable that the binding of $F_{81\text{-}101}$ to subunit B is a continuous process with the incoming C-terminus of F converting from a helical to an extended form and imparting perturbations that encourage the drift of ATP from site 1 towards site 2. A further tightening in the binding of $F_{81\text{-}101}$ with subunit B accompanies the migration of ATP from site 2 towards site 3. Once the ATP has occupied its final binding location (site 3), it is expected that $F_{81\text{-}101}$ undergoes a "loosening" from subunit B and goes back to adopting a helical structure. This anticipated loosening of $F_{81\text{-}101}$ is well reflected in the distribution of Cα distances between $F_{81\text{-}101}$ and subunit B (green line in Fig. S7). Unfortunately, this event is not adequately reflected in the binding energetics where the difference in enthalpy of binding between $F_{81\text{-}101}$ and subunit B, when nucleotide occupies site 2 and site 3, is negligible (Table S2). The complete binding and unbinding processes of $F_{81\text{-}101}$ to subunit B may occur at the millisecond timescale, while the scope of our study is to address the events immediately following 1) the conversion of the retracted state of $F_{81\text{-}101}$ to an elongated state and 2) binding to subunit B, when nucleotide is at site 1; and immediately preceding 1) the unbinding of $F_{81\text{-}101}$ from subunit B once the nucleotide has reached site 3 and 2) reconversion of the elongated $F_{81\text{-}101}$ to a retracted, helical form at the nanosecond timescale (Events summarized in Fig. 6).

In summary, the conformational and energetic coupling of the membrane bound A_O with the soluble A_3B_3 headpiece in archaeal ATP synthases has been addressed using a combination of experimental and theoretical methods. In a previous work (Raghunathan et al. 2010) we reconstructed the model of the subunit B-F complex of *M. mazei* Gö1 based on biochemical and tryptophan fluorescence spectroscopy derived distance restraints. This model shed light on how the A_1 and A_O motor elements of the ATP synthase interact with each other at the atomistic level. NMR, FCS, intrinsic tryptophan fluorescence spectroscopy, ITC and molecular dynamics simulations were employed to further extend this investigation to reveal, why this coupling of subunit B and F is of paramount importance for the suitable transfer of energy from A_O, via the stalk, to A_1 of the enzyme. Combining crystallography and molecular dynamics simulations in explicit solvent has revealed that the nucleotide, when bound to subunit B, occupies one of the two intermediate binding sites 1 and 2. Only upon the elongation and binding of the C-terminus of subunit F to the C-terminus of subunit B does the nucleotide migrate from site 1 via site 2 to its final binding site 3. When the nucleotide occupies site 2, the complex assumes a transition state like character and the large stabilization of site 3 occupation, compared to site 1 occupation (which actually undergoes a destabilization), appears to drive the reaction forward, i.e. the migration of ATP from site 2 to site 3.

Acknowledgments Drs. S. Gayen and A. Kumar are grateful to the authority of Nanyang Technological University for awarding research scholarship. This research was supported by A*STAR BMRC (08/1/22/19/576).

References

Brooks B, Karplus M (1983) Proc Natl Acad Sci U S A 80:6571–6575
Brooks BR, Brooks CL 3rd, Mackerell AD Jr, Nilsson L, Petrella RJ, Roux B, Won Y, Archontis G, Bartels C, Boresch S, Caflisch A, Caves L, Cui Q, Dinner AR, Feig M, Fischer S, Gao J, Hodoscek M, Im W, Kuczera K, Lazaridis T, Ma J, Ovchinnikov V, Paci E, Pastor RW, Post CB, Pu JZ, Schaefer M, Tidor B, Venable RM, Woodcock HL, Wu X, Yang W, York DM, Karplus M (2009) J Comput Chem 30:1545–1614
Butterfield SM, Waters ML (2003) J Am Chem Soc 125:9580–9581
Chang CE, Chen W, Gilson MK (2005) J Chem Theor Comput 1:1017–1028
Darden T, York D, Pedersen L (1993) J Chem Phys 98:10089–10093
DeLano WL (2002) The PyMOL molecular graphics system DeLano Scientific. Palo Alto, California
Dougherty DA (1996) Science 271:163–168
Dougherty DA (2007) J Nutr 137:1504–1508
Feller SE, Zhang YH, Pastor RW, Brooks BR (1995) J Chem Phys 103:4613–4621
Gallivan JP, Dougherty DA (1999) Proc Natl Acad Sci U S A 96:9459–9464
Gayen S, Vivekanandan S, Biuković G, Grüber G, Yoon HS (2007) Biochemistry 46:11684–11694
Grüber G, Marshansky V (2008) Bioessays 30:1096–1109
Grüber G, Svergun DI, Coskun U, Lemker T, Koch MH, Schägger H, Müller V (2001) Biochemistry 40:1890–1896
Hunke C, Chen WJ, Schäfer HJ, Grüber G (2007) Protein Expr Purif 53:378–383
Im W, Lee MS, Brooks CL 3rd (2003) J Comput Chem 24:1691–1702
Jorgensen WL, Chandrasekhar J, Madura JD, Impey RW, Klein ML (1983) J Chem Phys 79:926–935
Kneller DG, Goddard TD (1997) SPARKY, 3.105 ed. University of California, San Francisco
Kollman PA, Massova I, Reyes C, Kuhn B, Huo S, Chong L, Lee M, Lee T, Duan Y, Wang W, Donini O, Cieplak P, Srinivasan J, Case DA, Cheatham TE 3rd (2000) Acc Chem Res 33:889–897
Kumar A, Manimekalai MS, Grüber G (2008) Acta Crystallogr D: Biol Crystallogr D64:1110–1115
Kumar A, Manimekalai MS, Balakrishna AM, Hunke C, Weigelt S, Sewald N, Grüber G (2009) Proteins 75:807–819
Levitt M, Sander C, Stern PS (1985) J Mol Biol 181:423–447
Lolkema JS, Chaban Y, Boekema EJ (2003) J Bioenerg Biomembr 35:323–335
Mackerell AD Jr (2004) J Comput Chem 25:1584–1604
Mackerell AD Jr, Nilsson L (2008) Curr Opin Struct Biol 18:194–199
MacKerell AD Jr, Banavali N, Foloppe N (2000) Biopolymers 56:257–265

Manimekalai MS, Kumar A, Balakrishna AM, Grüber G (2009) J Struct Biol 166:38–45
Martyna GJ, Tobias DJ, Klein ML (1994) J Chem Phys 101:4177–4189
Müller V, Grüber G (2003) Cell Mol Life Sci 60:474–494
Numoto N, Kita A, Miki K (2004) Acta Crystallogr D60:810–815
Phillips JC, Braun R, Wang W, Gumbart J, Tajkhorshid E, Villa E, Chipot C, Skeel RD, Kale L, Schulten K (2005) J Comput Chem 26:1781–1802
Raghunathan D, Gayen S, Grüber G, Verma CS (2010) Biochemistry 49:4181–4190
R Development Core Team (2008) R Foundation for Statistical Computing, Vienna, Austria. ISBN 3-900051-07-0
Schäfer G, Engelhard M, Müller V (1999) Microbiol Mol Biol Rev 63:570–620
Schäfer I, Rössle M, Biuković G, Müller V, Grüber G (2006a) J Bioenerg Biomembr 38:83–92
Schäfer IB, Bailer SM, Düser MG, Börsch M, Bernal RA, Stock D, Grüber G (2006b) J Mol Biol 358:725–740
Seeber M, Cecchini M, Rao F, Settanni G, Caflisch A (2007) Bioinformatics 23:2625–2627
Sharp KA, Nicholls A, Fine RF, Honig B (1991) Science 252:106–109
Sitkoff D, Sharp KA, Honig B (1994) Biophys Chem 51:397–403
Srinivasan J, Miller J, Kollman PA, Case DA (1998) J Biomol Struct Dyn 16:671–682
Walker JE, Saraste M, Runswick MJ, Gay NJ (1982) EMBO J 1:945–951
Weber J, Senior AE (2003) FEBS Lett 545:61–70
Willis BTM, Pryor AW (1975) Thermal vibrations in crystallography. Cambridge University Press